Appl. Phys. B 82, 149–154 (2006)
DOI: 10.1007/s00340-005-2058-0

Applied Physics B
Lasers and Optics

Y.A. BAKHIRKIN[1]
A.A. KOSTEREV[1]
R.F. CURL[1]
F.K. TITTEL[1,✉]
D.A. YAREKHA[2]
L. HVOZDARA[2]
M. GIOVANNINI[2]
J. FAIST[2]

Sub-ppbv nitric oxide concentration measurements using cw thermoelectrically cooled quantum cascade laser-based integrated cavity output spectroscopy

[1] Rice Quantum Institute, Rice University, 6100 Main St., Houston, TX 77005, USA
[2] Institute of Physics, University of Neuchatel, 1 A.-L. Breguet, 2000 Neuchatel, Switzerland

Received: 11 August 2005/Revised version: 5 October 2005
Published online: 16 November 2005 • © Springer-Verlag 2005

ABSTRACT A nitric oxide (NO) gas sensor based on a thermoelectrically cooled, continuous-wave, distributed feedback quantum cascade laser operating at 5.45 μm (1835 cm^{-1}) and off-axis integrated cavity output spectroscopy combined with a wavelength-modulation technique was developed to determine NO concentrations at the sub-ppbv levels that are essential for a number of applications, such as medical diagnostics, environmental monitoring, and industrial process control. The sensor employs a 50-cm-long high-finesse optical cavity that provides an effective path length of ∼ 700 m. A noise equivalent (SNR = 1) minimum detection limit of 0.7 ppbv with a 1-s observation time was achieved.

PACS 07.07.Df; 33.20.Ea; 42.62.Fi; 87.64.Je

1 Introduction

The development of compact optical sensors for nitric oxide (NO) detection is of interest for a number of applications, such as environmental monitoring [1], atmospheric chemistry [2], industrial process control [3], combustion studies [4], and medical diagnostics [5, 6]. NO is involved in many vital physiological processes in the human body. For example, an elevated level of NO in exhaled air is correlated with airway inflammation in asthmatic patients. Knowledge of NO concentrations in the exhaled breath of these patients may allow health-care providers to adjust therapeutic drug dosages [7, 8]. For medical diagnostics purposes, it is essential to time resolve the NO concentration as a function of a breath-cycle phase, because the corresponding air samples originate in different parts of the respiratory tract. This application requires a sensor response time of ≤ 1 s and a NO minimum detection sensitivity of < 1 ppbv. Such high-sensitivity, rapid-response measurements are possible with laser absorption spectroscopy in the fundamental absorption band of NO.

Distributed feedback quantum cascade lasers (DFB QCLs) operating in a pulsed or continuous-wave (cw) mode are promising laser sources because of their narrow line widths, single-mode operation, tunability, power, reliability, and compactness. Until recently cw operation of QCLs was possible only at cryogenic temperatures and room-temperature (RT) operation was realized only with pulsed operation at low duty cycle, but recent developments in QCL technology now permit cw operation at around room temperature [9, 10].

A number of approaches utilizing QCLs for the optical sensing of trace NO have been reported. Background-free Faraday modulation spectroscopy has been demonstrated to be capable of measuring biogenic nitric oxide with a sensitivity of a few ppbv [11, 12]. Mid-infrared spectrometers based on a QCL and a multipass cell absorption platform achieve a minimum NO detection limit of ≤ 1 ppbv [1, 6, 13]. A technique based on cavity ring-down spectroscopy (CRDS) reaches a noise equivalent sensitivity at the sub-ppbv level in several seconds using a comparatively small sample volume because of a long optical path length obtained with ultra-high-reflectivity mirrors ($R \sim 99.99\%$) [14–16]. Another approach, which also uses such low-loss mirrors, is integrated cavity output spectroscopy (ICOS) [17, 18]. In 2001, an ICOS-based biogenic NO sensor utilizing a quantum cascade laser was reported by our group [19]. More recently, we demonstrated a noise equivalent sensitivity of 10 ppbv in 15 s for NO using a compact (∼ 5-cm long, ≤ 80-cm^3 volume) off-axis (OA)-ICOS cell and a liquid nitrogen (LN_2) cooled cw DFB QCL, operated at ∼ 5.2 μm [20]. The OA-ICOS approach, combined with a wavelength-modulation (WM) technique, showed a five-fold sensitivity enhancement with the same data-acquisition time. Silva et al. [21] obtained a minimum detection sensitivity of < 1 ppbv in 4 s for NO in human breath using an ICOS cell and a thermoelectrically cooled (TEC) pulsed QCL.

In this work we use a novel and now commercially available TEC, cw, DFB quantum cascade laser fabricated by the collaborating team from the University of Neuchatel, Switzerland [9]. The DFB cw QCL characteristics, such as a narrow laser spectral width (≤ 3 MHz [16], necessary for efficient laser to cavity coupling) and high average power make cw TEC QCLs more suitable than pulsed QCLs for ICOS-based sensor platforms for real-world applications, avoiding the size and complications of liquid-nitrogen cooling required by earlier QC lasers. The basic sensor platform is an OA-ICOS configuration with a 50-cm-long optical cavity. A wavelength-modulation technique (harmonic detection) was implemented in order to reach sub-ppbv levels of detection sensitivity.

✉ Fax: 713-348-5686, E-mail: fkt@rice.edu

2 Description of the sensor platform

A schematic of the ICOS-based sensor is depicted in Fig. 1. A TEC cw DFB QCL, operating at 5.45 μm [9], was installed in a compact evacuated QCL housing. The housing was equipped with a 25-mm-diameter CaF_2 window and a single-stage thermoelectric cooler (Melcor Corporation, type UT8-12-40F1) that provides thermal control of the QC laser. A minimum QCL temperature of −32 °C can be achieved when the laser housing is at reduced pressures (typically $\sim 10^{-3}$ to 10^{-4} Torr) and the hot side of the TEC is actively water cooled. A three-lens collimator (see Fig. 1) was employed to achieve optimum coupling of the QCL radiation to the OA-ICOS cavity. The first lens after the QCL is a 25-mm-diameter ZnSe aspherical lens with an antireflection coating, and a 12.7-mm effective focal length. This reduces spherical aberration thereby improving the quality of the beam coupled to the OA-ICOS cell. An iris diaphragm in the focal point of the second lens serves as a spatial optical filter to minimize fringes caused by the collimator lenses and the laser housing output window, as well as reducing back reflection to the QCL by a factor of five. The second and third lenses also have diameters of 25 mm and effective focal lengths of 500 mm and 63 mm, respectively. The collimated QCL beam incident on the OA-ICOS cavity has a diameter of 2.3 mm. Highly reflective 50.8-mm-diameter concave mirrors (1-m radius of curvature) separated by a 50-cm stainless steel spacer form the optical OA-ICOS cavity. The same set of mirrors that was used in our previous study at a frequency of 1920 cm^{-1} (5.2 μm) [20] was employed in this work. The reflection coefficient for the ultra-low-loss mirror set at 1920 cm^{-1} was estimated to be $R \geq 99.975\%$ using a CDRS approach [20]. According to the mirror specifications the reflection coefficient at a laser frequency of 1836 cm^{-1}, which was used in the current study, is the same (with a discrepancy of ±0.005%) according to the manufacturer (Los Gatos Research, Inc.). The longer cavity length of 50 cm was chosen in order to enhance the NO detection limit of the OA-ICOS technique. The cavity was aligned off-axis with respect to the laser beam providing improved cavity mode noise suppression. The suppression of cavity mode noise is the critical factor determining the sensitivity of the ICOS technique [18, 20]. Further mode noise suppression sensitivity enhancement was obtained by averaging the cavity resonances by dithering the cavity length using an assembly of three piezo-electric actuators attached to one of the resonator mirrors (see Fig. 1). The mirror was moved back and forth with a frequency of ∼ 200 Hz and a maximum translation travel of ∼ 15 μm.

The cw QCL utilized in this work was a 3-mm-long, 14-μm wide, junction-up-mounted DFB laser with a high-reflection coating evaporated on its back facet. The spectral output, current and temperature tuning ranges, as well as tuning rades rate of the QCL used in this work were evaluated using

1. a 10-cm reference cell filled with a calibration mixture of $NO + N_2$;
2. an air-spaced Fabry–Pèrot etalon, which consists of two wedged ZnSe windows;
3. HITRAN database simulated spectra, which were compared with the experimental results.

The laser operated at temperatures of up to +20 °C with a total tuning range from ∼ 1827 cm^{-1} (+20 °C) to ∼ 1838 cm^{-1} (−32 °C). The temperature-tuning rate was ∼ 0.2 cm^{-1}/K. A temperature controller (Wavelength Electronics, Inc., model MPT-10000) provides a long-term temperature stability δT of ≤ 0.01 °C, limiting the spectral line shift to ≤ 0.002 cm^{-1}, which is negligible compared to the NO line width at 200 Torr (0.032 cm^{-1}). At a fixed temperature of the laser thermal sink, the frequency of the output radiation can be tuned by varying the QCL current. A current driver (Wavelength Electronics, Inc., model MPL-2500) was used to operate the QCL. Temperature and current spectral tuning ranges of the QCL are depicted in Fig. 2 together with a HITRAN-based simulated absorption spectrum of an $NO - N_2$ mixture.

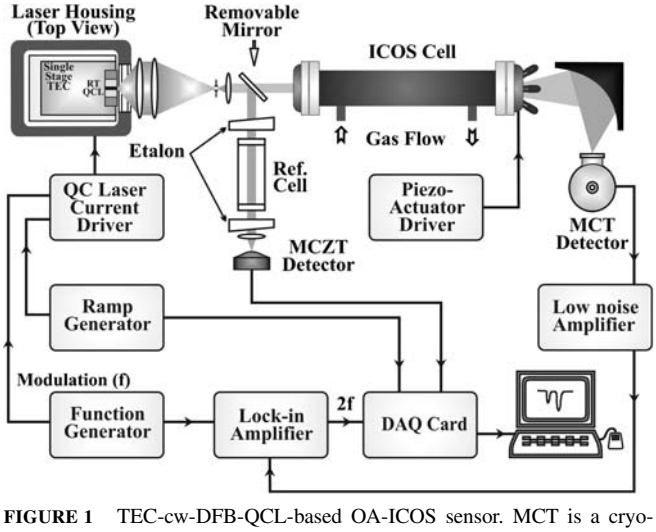

FIGURE 1 TEC-cw-DFB-QCL-based OA-ICOS sensor. MCT is a cryogenically cooled photovoltaic HgCdTe detector and MCZT is a thermoelectrically cooled HgCdZnTe photodetector (Vigo System, model PVMI-10.6)

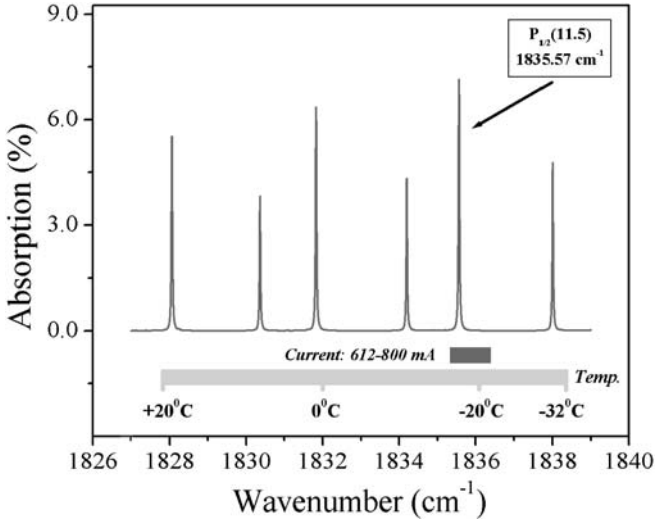

FIGURE 2 HITRAN-based simulation of an absorption spectrum for a NO–N_2 mixture in the tuning range of a TEC-cw-DFB QCL operating at 5.45 μm. The total pressure of the mixture is 200 Torr; path length is 700 m; concentration of NO is 94.9 ppbv. The NO absorption line $P_{1/2}(11.5)$ at 1835.57 cm^{-1} (denoted by the *arrow*) was used for the concentration measurements reported in this work

The combined NO absorption line $P_{1/2}(11.5)$, which is a superposition of two lambda doubling components centered at 1835.57 cm^{-1}, was selected for concentration measurements as it is the most intense line in the QCL tuning range. A strong interference from H_2O throughout the entire spectral output range of the QCL can be avoided by using a commercially available Nafion dryer assembly (Perma Pure LLC) with an appropriate length and flow rate to meet breath-analysis requirements. The $P_{1/2}(11.5)$ line was reached at a temperature of −21 °C and a current of ∼ 778 mA. Two function generators (Stanford Research Systems, model DS345) were utilized for QCL current ramping and for frequency modulation in applying the wavelength-modulation (WM) technique. The QCL ramp and WM frequencies were ∼ 1 kHz and ∼ 50 kHz, respectively.

The ICOS cavity output signal was focused onto a LN_2-cooled photovoltaic HgCdTe detector with a built-in transimpedance preamplifier (Kolmar Technologies, model KMPV8-1-J1/DC) by means of an off-axis aluminum parabolic mirror. After additional amplification (gain factor was 10^3) and filtering (low-pass filter was set to 1 MHz) by a low-noise amplifier (Stanford Research Systems, model SR560), the detector signal was fed into a lock-in amplifier (Stanford Research Systems, model SR 830) for second-harmonic ($2f$) processing. The output of the lock-in amplifier was acquired by a data-acquisition card installed in a PC using LabView 7.1. After further averaging, the data is stored in preparation for fitting. Initial feasibility NO concentration measurements with a long cell were made without the wavelength-modulation technique. In this case the amplified photodetector signal was directed straight to the data-acquisition card.

The measured laser radiation power after the three-lens collimator system when the QCL was operated at −21 °C is plotted in Fig. 3 as a function of QCL drive current. Single-mode lasing started at a threshold of 608 mA and continued up to 624 mA with a slope efficiency of ∼ 1.9 mW/A. A power kink was observed at ∼ 624 mA caused by the onset of a second laser mode. This behavior results from insufficient mode suppression by the DFB structure of the QCL and has been corrected in very recent thermoelectrically cooled DFB QCLs [10]. The spectral range, which corresponds to a current from 624 to 800 mA, was studied at −21 °C (as the two-mode behavior depends on temperature) in order to characterize the power of each mode. This study was necessary because total absorption of one laser mode does not result in zero detector signal. The coexistence of two laser modes, which are frequency shifted from each other, resulted in additional spectral features ('false' lines) as the absorption spectra from two modes were overlapped. However, quantitative concentration measurements were possible because the frequency and the power of each mode were well defined and reproducible at a certain QCL temperature. The frequency of each mode changes almost linearly with current. The total QCL power with a slope efficiency of ∼ 8.5 mW/A includes inputs from two modes: a 'weak' mode with a threshold of 608 mA and a tuning rate of 4.9 cm^{-1}/A, and a 'strong' mode with a threshold of 624 mA, a tuning rate of 5.7 cm^{-1}/A, and a slope efficiency of ∼ 6.6 mW/A. The frequency shift between the two modes was 0.39 cm^{-1} at 778 mA with the 'weak' mode having the higher frequency. All NO concentration measurements were made using the 'strong' QC laser mode, which covers a frequency range from 1835.3 to 1836.4 cm^{-1} by current scanning. The QC laser line width was estimated to be ∼ 35 ± 3 MHz and was determined mainly by the current ripple on the QCL driver current source.

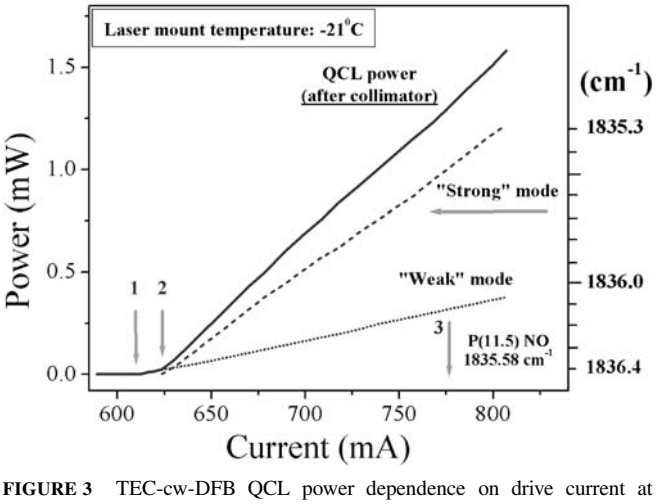

FIGURE 3 TEC-cw-DFB QCL power dependence on drive current at a laser submount temperature of −21 °C. The QCL power was measured in front of the ICOS cavity. *Arrows* 1 and 2 indicate the laser threshold at 608 mA and the onset of a second laser mode at 624 mA, respectively. *Arrow* 3 represents the required QCL driver current (778 mA) to obtain the selected NO line at 1835.57 cm^{-1}. The frequency scale used is for the 'strong' mode

3 Experimental results

A calibration mixture (Scott Specialty Gases, Inc.) of 94.9 ppbv NO in N_2 as the balance gas was used for the evaluation of the QCL-based NO sensor system. The NO concentration was certified by the supplier using a chemiluminescence technique (NO analyzer by GE Analytical Instruments, formerly Sievers). A diluter was used to obtain up to five times lower NO concentration levels. Measurements were made at a constant flow rate of ∼ 100 sccm as adhesion to the ICOS cavity walls may affect the precision and accuracy of the NO concentration measurements. Pressure levels were varied from 50 to 200 Torr. A gas-flow system described in detail in [20] was utilized for measurement pressure and flow control.

In a previous study [20] a stable 5.3-cm-long two-mirror OA-ICOS cavity geometry was used for NO concentration measurements. The minimum detectable concentration was 2 ppbv in 15 s at ∼ 5.2 μm with a laser power of ∼ 20 mW and mirror losses of 250 ppm. Replacement of a LN_2-cooled QCL by the TEC QCL described in Sect. 2 in the same OA-ICOS architecture leads to a higher NO detection limit, because there is ∼ 20 times less available mid-IR laser power. Hence, to obtain target NO concentration levels of ≤ 1 ppbv, it was necessary to increase the physical length of the ICOS cavity to 50 cm in order to enhance the effective optical path length. The cavity gain factor $G = R/(1 - R)$ is ∼ 4000 for a pair of ICOS mirrors assuming that the reflectivity R is ∼ 99.975% at 5.45 μm (1836 cm^{-1}) [18]. In order to ensure that the measured absorption is linear with respect to NO concentration after increasing the cavity length to 50 cm, the

condition $G\alpha \ll 1$ (i.e. weak-absorption limit) should be satisfied, where α is the single-pass absorption. For a maximum NO concentration of 94.9 ppbv the factor $G\alpha$ is ~ 0.2. This means that for smaller NO concentrations the amplitude of the absorption signal scales linearly with concentration values.

Initial NO concentration measurements with the 50-cm-long ICOS cell were made without applying wavelength modulation. The QC laser output was scanned by current with a frequency of 1 kHz across the absorption line. The cavity output signal was sampled, averaged, and processed using a data-acquisition card and a PC. The results are depicted in Fig. 4. The solid curve shows a 94.9 ppbv NO absorption line obtained from averaged ICOS signals. An absolute value of the absorption was obtained taking into account an offset resulting from the bimodal characteristic of the QCL (see Sect. 2 and Fig. 3). The number of acquired averages of spectra was 1000 and the typical data-acquisition time was 1 s. The dotted line represents a Voigt fit with parameters: Lorentzian width of $\sim 2.61 \times 10^{-2}\,\mathrm{cm}^{-1}$ that is in good agreement with the HITRAN predicted value of $2.63 \times 10^{-2}\,\mathrm{cm}^{-1}$ and a Gaussian line width of $\sim 0.41 \times 10^{-2}\,\mathrm{cm}^{-1}$ determined by the temperature of the gas. Comparison between fitted data and HITRAN simulated spectra yielded an effective optical path length of 700 m provided that $G\alpha \ll 1$ and the line shape obeys a Voigt profile at 200 Torr. This is in good agreement with our previous results for a compact 5.3-cm-long cell obtained with the same set of mirrors that provided a 75-m effective optical path length. The effective optical path length scales with the physical length of the ICOS cavity. The discrepancy between the measured (~ 700 m) and theoretical (~ 2000 m) effective optical path lengths of the OA-ICOS derived from the cavity ring-down time is due to several factors such as: (1) non-homogeneity of the reflectivity across the 2-in-diameter mirror surfaces and therefore an uncertainty of the cavity decay time, (2) a large number of higher-order transverse modes that are involved in OA-ICOS-based gas measurements with higher diffraction losses than for the TEM_{00} mode, which leads to a decrease of the effective optical path length, and (3) tilting of the piezo-electric-driven mirror which affects the OA-ICOS cavity alignment and therefore results in a decrease of the cavity finesse.

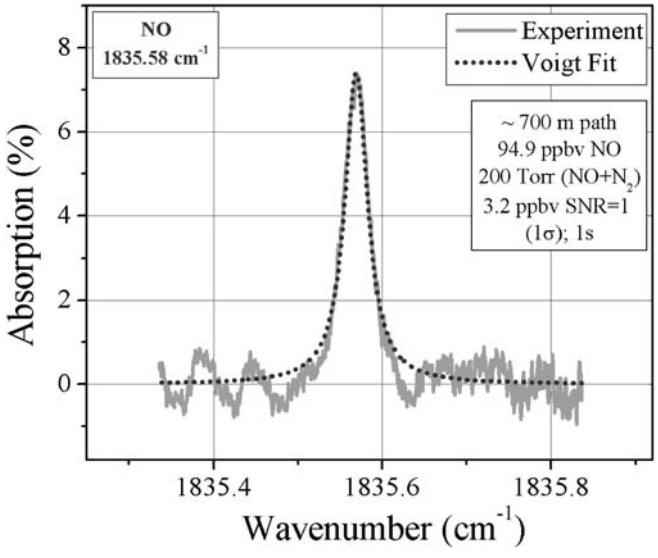

FIGURE 4 Measured OA-ICOS spectrum of a 94.9 ppbv NO:N_2 calibration mixture fitted by a Voigt function. Fit parameters: Lorentzian line width is $\sim 2.61 \times 10^{-2}\,\mathrm{cm}^{-1}$ that is in good agreement with a HITRAN predicted value of $2.63 \times 10^{-2}\,\mathrm{cm}^{-1}$, Gaussian (Doppler) width is $\sim 0.41 \times 10^{-2}\,\mathrm{cm}^{-1}$. Minimum detectable NO concentration is 3.2 ppbv, obtained from the deviation of the area under the absorption curve δA. Time constant (data-acquisition time) is 1 s

The principal limitation of the OA-ICOS detection sensitivity is the residual cavity mode noise that results from incomplete averaging of the cavity transmission resonances. Additional constraints are imposed by optical fringes caused by accidental low-finesse etalons resulting from spurious reflections in the optical path. Some of these fringes are apparent in Fig. 4. We have compared the normal dispersion σ of the averaged output of an evacuated cavity during a QCL scan (output was normalized to the laser power) for 10^3 and 10^6 averages (data-acquisition time was from 1 to 10^3 s, accordingly). σ does not obey the $1/N^{1/2}$ rule and decreases only ~ 6 times instead of ~ 30 due to incomplete cancelation of the optical fringes. For NO concentration measurements the number of averages was limited to 10^3 to obtain a sensor response time of 1 s at a ramp frequency of 1 kHz. An estimate for the NO detection limit was obtained from the standard deviation of the area δA under a Voigt data fit using the equation derived in [16]:

$$\delta A \approx \sigma \left[\frac{\Delta\nu}{\int g^2(\nu)\,\mathrm{d}\nu} \right]^{1/2}, \qquad (1)$$

where $g(\nu)$ is a line-shape envelope normalized to unit area, σ is the standard error for the residual between the actual experimental absorption line and the fitted curve, and $\Delta\nu$ is the spacing between experimental points. For a Lorentzian line shape this equation becomes $\delta A = \sigma(\pi\Delta\nu w)^{1/2}$, where w denotes the FWHM of the line envelope. Assuming that the Voigt line shape reduces to a Lorentzian line shape at 200 Torr, an estimate for the noise equivalent sensitivity of 3.2 ppbv in 1 s was obtained.

In order to improve sensitivity towards the NO target limit of ≤ 1 ppbv required for breath analysis, wavelength-modulation spectroscopy (WMS) [13, 22–25] was added to the OA-ICOS-based sensor platform. In this case, the QCL current is modulated at a high frequency ν, and the wavelength is tuned slowly across the spectral line of interest by means of a current ramp with a frequency Ω ($\nu \gg \Omega$). The detector output is processed by a lock-in amplifier referenced to the modulation frequency $1f$ or $2f$ (first- and second-harmonic detection, respectively). This type of detection results in a significant improvement in the signal-to-noise-ratio (SNR) [22]. The amplitude of a WMS-based signal scales linearly with gas concentration [23], which facilitates calibration and a quantitative gas-concentration measurement.

The OA-ICOS-based sensor can also benefit from applying WMS as reported in [20, 26, 27]. In the present work the WMS parameters (amplitude, modulation frequency, and modulation function) and the gas pressure inside the ICOS cavity were optimized in order to maximize the signal. Sinusoidal modulation at ν together with a triangular ramp at Ω was found to result in the optimum SNR. The frequencies were $\Omega = 1$ kHz and $\nu = 50$ kHz, respectively. The lock-in

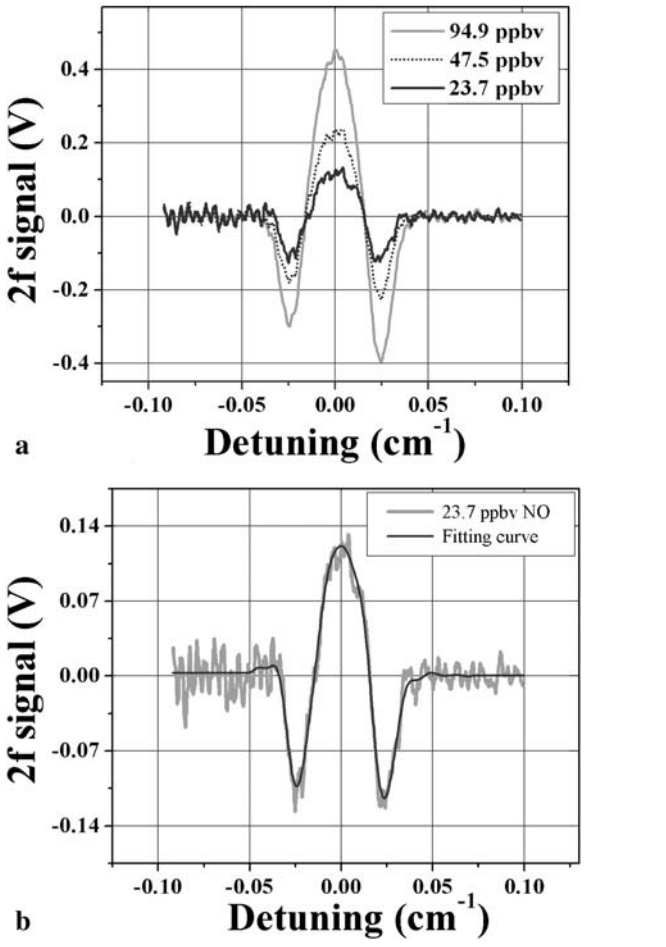

FIGURE 5 (**a**) Averaged second-harmonic scan of the ICOS cavity output for the NO absorption line $P_{1/2}(11.5)$ at 1835.57 cm^{-1} (5.45 μm) for three concentrations. Data-acquisition time is 1 s. (**b**) Averaged measured ($2f$) signal for a NO concentration of 23.7 ppbv and fitting curve, obtained using a general linear fitting procedure [28]. The standard deviation σ of the fit coefficients corresponds to 0.7 ppbv

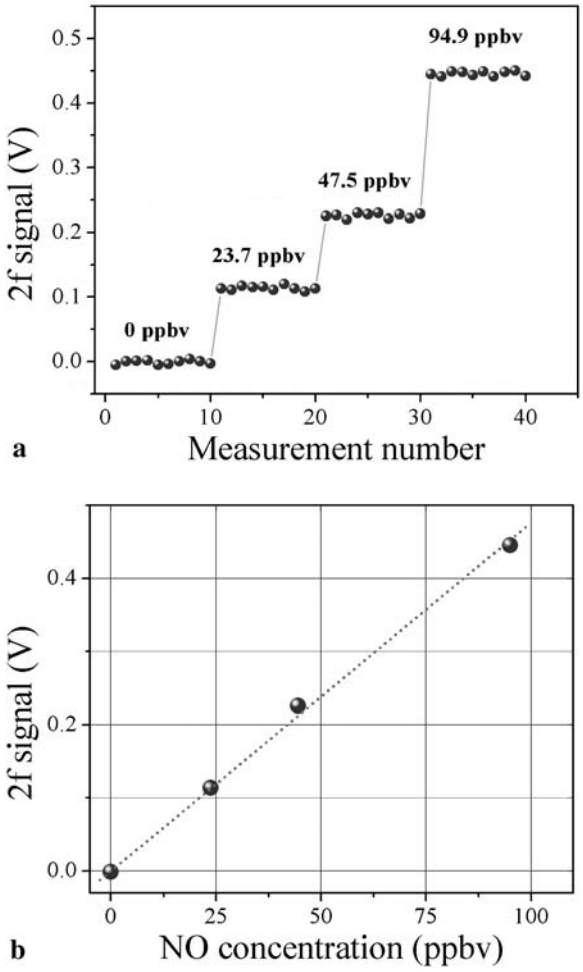

FIGURE 6 $2f$ NO concentration measurements for three concentrations in flow conditions. A commercial 94.9 ppbv NO in N_2 calibration mixture was diluted to a level of 23.7 ppbv. (**a**) Experimental data for four sets of measurements. (**b**) A linear curve is obtained from the measured ($2f$) amplitudes and known NO concentration levels

amplifier output was averaged using a data-acquisition card and LabView-based software. Examples of averaged WMS signals for three NO concentrations are presented in Fig. 5a. The number of averages was set to 10^3. The basic calibration mixture with a NO concentration of 94.9 ppbv was diluted four-fold. A WMS signal for a calibrated NO concentration of 23.7 ppbv was fitted using a general linear fit procedure [28] as shown in Fig. 5b. A 1σ deviation of the amplitude obtained as a fit result corresponds to 0.7 ppbv. Step concentration measurements of NO are depicted in Fig. 6a. Each measurement was repeated 10 times and the amplitude of the WMS signal was retrieved and plotted in Fig. 6a. An additional set of 10 points was obtained by analyzing the baseline behavior (zero concentration of NO). Using this procedure the 1σ variation in NO was also found to be ~ 0.7 ppbv. Furthermore, the amplitudes of the ($2f$) signals obtained from the curve fittings scale linearly with the NO concentration (see Fig. 6b). The ~ 5 times improved NO detection sensitivity obtained using WMS is due by the insensitivity of the $2f$ signal to low-frequency baseline variations and suppression of the photodetector low-frequency noise and zero-level drift.

4 Conclusions

An OA-ICOS-based NO sensor, which exploits the recent availability of a cw TEC DFB QCL operating at 5.45 μm and a 50-cm-long high-finesse optical cavity, demonstrated the feasibility to detect and quantify NO concentrations at a level of ≤ 1 ppbv in 1 s. The application of off-axis alignment of the ICOS cavity and simultaneous modulation of the cavity length by piezo-electric actuators leads to minimization of the output intensity fluctuations induced by the cavity resonance, while preserving the extension of the effective optical path in the absorbing target gas. It has been shown that the OA-ICOS technique yields a minimum NO detection sensitivity of ~ 3 ppbv in 1 s. A combination of OA-ICOS and a $2f$ WMS technique leads to minimum NO detection levels of ~ 0.7 ppbv. Additional improvement in sensitivity can be obtained by using a more powerful (~ 50 mW) single-frequency cw QCL [10] operating at 1900.1 cm^{-1} (optimum frequency for interference-free NO detection [21]) and recently available 50 ppm ultra-low-loss mirrors (instead of the 250 ppm mirrors used in this work).

ACKNOWLEDGEMENTS Financial support of the work performed by the Rice group was provided by the National Aeronautics and Space Administration (NASA), NASA Contract No. NAS2-92038 via a subaward from Physical Sciences Inc. (PSI), the Texas Advanced Technology Program, the Robert Welch Foundation, and the Office of Naval Research via a subaward from Texas A&M University. The work performed at the University of Neuchatel, Switzerland was partially supported by the Swiss National Science Foundation NCCR 'Quantum photonics' as well as by funding from the European Union project 'ANSWER'.

REFERENCES

1 D.D. Nelson, J.H. Shorter, J.B. McManus, M.S. Zahniser, Appl. Phys. B **75**, 343 (2002)
2 J.H. Steinfeld, S.N. Pandis, *Atmospheric Chemistry and Physics: From Air Pollution to Climate Change* (Wiley, New York 1998)
3 G. Wysocki, A.A. Kosterev, F.K. Tittel, Appl. Phys. B **80**, 617 (2005)
4 H. Gupta, L.-S. Fan, Ind. Eng. Chem. Res. **42**, 2536 (2003)
5 C. Roller, K. Namjou, J.D. Jeffers, W. Potter, P.J. McCann, J. Grego, Opt. Lett. **27**, 107 (2002)
6 C. Roller, K. Namjou, J.D. Jeffers, M. Camp, A. Mock, P.J. McCann, J. Grego, Appl. Opt. **41**, 6018 (2002)
7 A. Amann, D. Smith (eds.), *Breath Analysis for Clinical Diagnosis and Therapeutic Monitoring* (World Scientific, Singapore 2005), pp. 75–84
8 A.D. Smith, D.R. Taylor, Curr. Opin. Allergy Clin. Immunol. **5**, 49 (2005)
9 S. Blaser, D.A. Yarekha, L. Hvozdara, Y. Bonetti, A. Miller, M. Giovannini, J. Faist, Appl. Phys. Lett. **86**, 041 109-1 (2005)
10 S. Blaser, Y. Bonetti, L. Hvozdara, A. Mueller, Quantum-cascade lasers for TDLS. In *5th International Conference on Tunable Diode Laser Spectroscopy*, Florence, Italy, 11–15 July 2005
11 H. Ganser, W. Urban, J.M. Brown, Mol. Phys. **101**, 545 (2003)
12 H. Ganser, M. Horstjann, C.V. Suschek, P. Hering, M. Mürtz, Appl. Phys. B **78**, 513 (2004)
13 W.H. Weber, T.J. Remillard, R.E. Chase, J.F. Richert, F. Capasso, C. Gmachl, A.L. Hutchinson, D.L. Sivco, J.N. Baillargeon, A.Y. Cho, Appl. Spectrosc. **56**, 706 (2002)
14 B.A. Paldus, C.C. Harb, T.G. Spence, R.N. Zare, C. Gmachl, F. Capasso, D.L. Sivco, J.N. Baillargeon, A.L. Hutchinson, A.Y. Cho, Opt. Lett. **25**, 666 (2000)
15 B.A. Paldus, A.A. Kachanov, Spectroscopic techniques: cavity-enhanced methods. In *Atomic, Molecular, and Optical Physics Handbook*, Part C: *Molecules*, ed. by G.W.F. Drake (Springer, Berlin 2005), Chap. 43, p. 621
16 A.A. Kosterev, A.L. Malinovsky, F.K. Tittel, C. Gmachl, F. Capasso, D.L. Sivco, J.N. Baillargeon, A.L. Hutchinson, A.Y. Cho, Appl. Opt. **40**, 5522 (2001)
17 A. O'Keefe, J.J. Scherer, J.B. Paul, Chem. Phys. Lett. **307**, 343 (1999)
18 J.B. Paul, L. Larson, J.G. Anderson, Appl. Opt. **40**, 4904 (2001)
19 L. Menzel, A.A. Kosterev, R.F. Curl, F.K. Tittel, C. Gmachl, F. Capasso, D.L. Sivco, N.J. Baillargeon, A.L. Hutchinson, A.Y. Cho, W. Urban, Appl. Phys. B **72**, 859 (2001)
20 Y.A. Bakhirkin, A.A. Kosterev, C. Roller, R.F. Curl, F.K. Tittel, Appl. Opt. **43**, 2257 (2004)
21 M.L. Silva, D.M. Sonnenfroh, D.I. Rosen, M.G. Allen, A. O'Keefe, Appl. Phys. B **81**, 705 (2005)
22 J. Reid, D. Labrie, Appl. Phys. B **26**, 203 (1981)
23 D.S. Bomse, A.C. Stanton, J.A. Silver, Appl. Opt. **31**, 718 (1992)
24 K. Namjou, S. Cai, E.A. Whittaker, J. Faist, C. Gmachl, F. Capasso, D.L. Sivco, A.Y. Cho, Opt. Lett. **23**, 219 (1998)
25 E.L. Wilson, J.H. Miller, Meas. Sci. Technol. **12**, 1701 (2001)
26 V.L. Kasyutich, C.E. Canosa-Mas, C. Pfrang, S. Vaughan, R.P. Wayne, Appl. Phys. B **75**, 755 (2002)
27 A. Zybin, Y.A. Kuritsyn, V.R. Mironenko, K. Niemax, Appl. Phys. B **78**, 103 (2004)
28 A.A. Kosterev, F.K. Tittel, R. Köhler, C. Gmachl, F. Capasso, D.L. Sivco, A.Y. Cho, S. Wehe, M.G. Allen, Appl. Opt. **41**, 1169 (2002)